Chapter 8

Analysis of Kinetics Parameters Controlling Atomistic Reaction Process of a Quasi-Reversible Electrode System

Yuji Imashimizu

Additional information is available at the end of the chapter

http://dx.doi.org/10.5772/51896

1. Introduction

For understanding the mechanism of electrolysis it is important to estimate kinetics parameters controlling the atomistic reaction process of metal electrode that is polarized in an electrolyte solution, but it seems not to have been performed satisfactorily. The reason for this is attributed to the fact that because actual electrode reactions proceed quasi-reversibly via consecutive two processes which consist of surface reaction and volume diffusion of ions involved in the reaction, the expression for its current density/overpotential relationship have become complex and not been presented explicitly. This is also related to the subjects of studies concerning the process of deposition or dissolution of atoms in crystal growth or its dissolution.

It is well known that the etch pits having a crystallographic symmetry are formed at dislocation sites of the low indices surfaces of a crystal which was etched under a specified condition (e.g. Gilman et al., 1958; Young, Jr., 1961). The dislocation etch pit is thought to be formed via a nucleation and growth process of two-dimensional pits at the dislocation site or via a spiral dissolution of the surface step which is caused by screw dislocation (Burton et al., 1951; Cabrela and Levine, 1956). Therefore elucidation of its formation mechanism is important for understanding of the surface step motion which is thought to play major role in the dissolution process of a crystal, and dissolution kinetics of crystals in the etch pit formation has been investigated and discussed by some researchers (e.g. Ives and Hirth, 1960; Schaarwächter, 1965; Jasper and Schaarwächter ,1966; Van Der Hoek et al., 1983) so far.

However the research concerning parameters controlling surface step motion in the dissolution of crystals has not been satisfactorily performed. Especially it has not been examined quantitatively except for a few studies (e.g. Onuma, 1991). This is principally due

to the reason that because the dissolution of a crystal proceeds generally via a dissolution reaction of surface atom and diffusion process of the dissolved atom (ion) into interior of solution, it is difficult to experimentally inspect the dissolution kinetics of surface step which depends on both processes. Since the dissolution rate of a metal crystal which is anodically dissolved under polarization in an electrolyte solution can be investigated by measurement of current density, dissolution mechanism of metal crystals has been researched electrochemically (e.g. Despic and Bockris, 1960; Lee and Nobe, 1986). However because of the same reason as the above mention, discussions on the results have become complex and not always contributed to understanding of surface step motion.

Recently, however, it has been proposed by the author that an expression to analyze the relationship between anodic current density and overpotential of a quasi-reversible electrode system including both the consecutive reaction processes is derived explicitly on the basis of an appropriate assumption (Imashimizu, 2010, 2011). According to the analysis, if the anodic and cathodic diffusion-limited current densities are measured for a given quasi-reversible electrode system, we can experimentally determine the kinetics parameters controlling dissolution process of crystals of the metal electrode, by assuming expressions for the activation and concentration overpotentials which are driving forces of surface reaction process and volume diffusion process respectively.

Thus the dissolution rates at dislocation-free and edge dislocation sites of (111) surface when a copper crystal was anodically dissolved in an electrolyte solution are investigated and discussed based on the above thinking, in this chapter. The relationships between anodic current density and overpotential are analyzed and discussed electrochemically by using the method developed for anodic dissolution processes of quasi-reversible electrode as described above. Activation enthalpy, transfer coefficient and surface concentrations of the ions involved in the dissolution process are experimentally estimated, and kinetics parameters controlling anodic reaction of the copper crystal/electrolyte system are quantitatively examined. An expression for the vertical dissolution rate at dislocation site is proposed based on a nucleation model of two-dimensional pit, and the critical free energy change at nucleation is quantitatively examined.

2. Experimental procedures for study of dissolution kinetics of copper crystals

2.1. Preparation of specimens

Single crystals of copper with [111] direction about 10 mm in diameter were prepared from the starting material of re-electrolyzed copper of 99.996 % purity by using the pulling method. They were divided into the cylindrical crystals approximately 15 mm length by a strain-free cutting. A terminal for detection of electric current and potential was soldered to an end surface of the cylindrical crystals. Another end surface was chemically polished so that the deviation of surface orientation from [111] direction is within 8.7×10^{-3} rad, and was further electrolytically polished in a high concentrated phosphoric acid solution. The crystal

specimen was embedded in a Teflon holder with paraffin so that its polished surface is exposed. Then it was supplied for the electrolysis experiment after the boundary portion between the paraffin and the periphery of polished surface was covered with a vinyl seal having a hole 6 mm in diameter (Watanabé et al., 2003).

2.2. Apparatus for potentiostatic electrolysis

Schematic diagram of the electrolytic cell for this experiment is shown in Fig.1 (Watanabé et al., 2003). The crystal specimen was immersed in the electrolyte solution which consists of 5 kmol m^{-3} NaCl, 0.25 kmol m^{-3} NaBr and 10^{-4} kmol m^{-3} CuCl (Jasper and Schaarwächter, 1966) so that (111) surface of copper is located at approximately 5mm below the surface of electrolyte solution, and was held at a specified temperature. Then, the crystal specimen was set under a constant overpotential, and (111) surface of the crystal was anodically dissolved for a prescribed time, while anodic current density/time curve was recorded. The potentiostatic electrolysis experiments were performed at a range of lower overpotential and at a range of higher overpotential. After that the structure of dissolved surfaces were observed by use of the optical microscope system equipped with lens for interferometry.

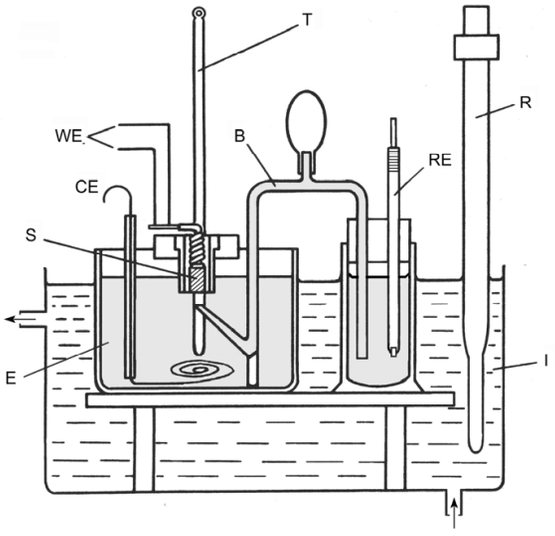

Figure 1. Schematic diagram of electrolytic cell. S: sample; E: electrolyte; WE: terminal for potential and current; RE: saturated calomel electrode; CE: counter electrode of platinum wire; B: salt bridge; I: thermobath; R: Regulator; and T: thermometer.

2.3. Features of anodic current density/time curves and structure of dissolved surface

Figure 2 shows typical anodic current density/time curves which were recorded while the copper crystal was anodically dissolved for 360 s or 600 s at the respective overpotentials. Anodic current density under any condition decreases steeply immediately after start of electrolysis and reaches a nearly constant current density i_s when it was carried out at an

overpotential lower than about 125 mV as shown by the curve of 87 mV in Fig.2. Figures 3 (a), (b) and (c) are the optical micrographs of the (111) surfaces which were dissolved for 600 s at overpotentials in a range of 60 mV to 125 mV being held at 298K. The surfaces are rather smooth though etch pits tend to be formed as overpotential increases.

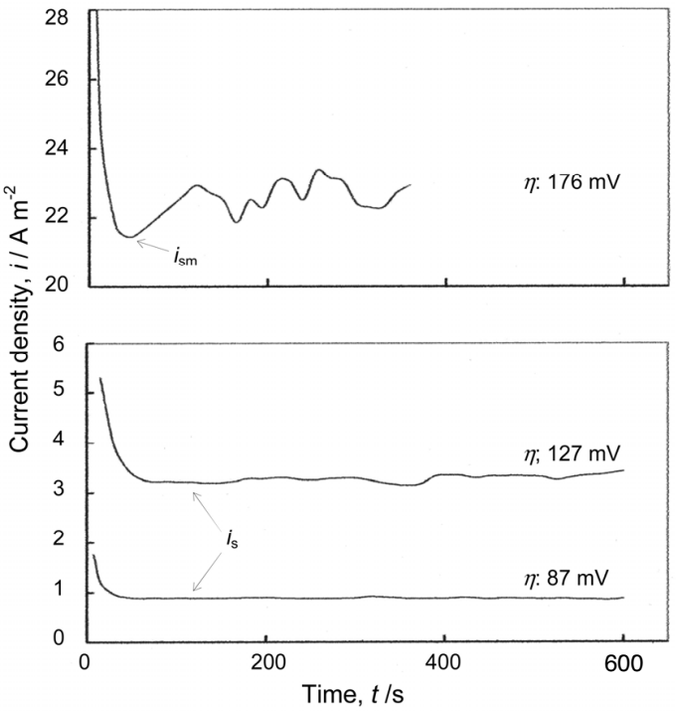

Figure 2. Anodic current density/time curves under potentiostatic electrolysis at 298K.

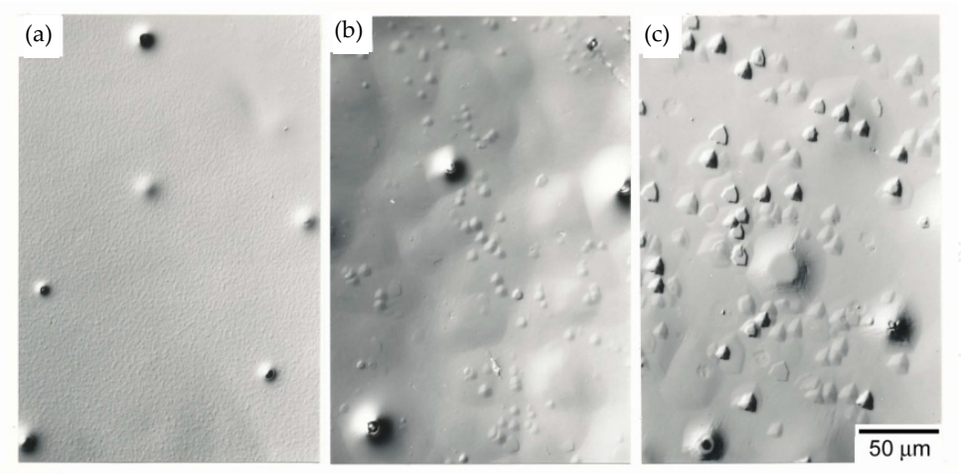

Figure 3. Optical micrographs of the surfaces which were anodically dissolved at lower overpotentials of (a): 58 mV, (b): 88 mV, and (c): 108 mV.

On the other hand, the current density reaches a minimum current density i_{sm} that is pointed by arrow after the initial steep decrease when an overpotential higher than about 125 mV was applied. Then it tends to increase gradually along with fluctuating and take a higher steady value as shown by the curve of 176 mV. Figures 4 (a), (b), and (c) are optical

micrographs of the surfaces which were dissolved for 300 s at 156, 166, and 176 mV respectively being held at 298K. One can see that etch pits are significantly formed.

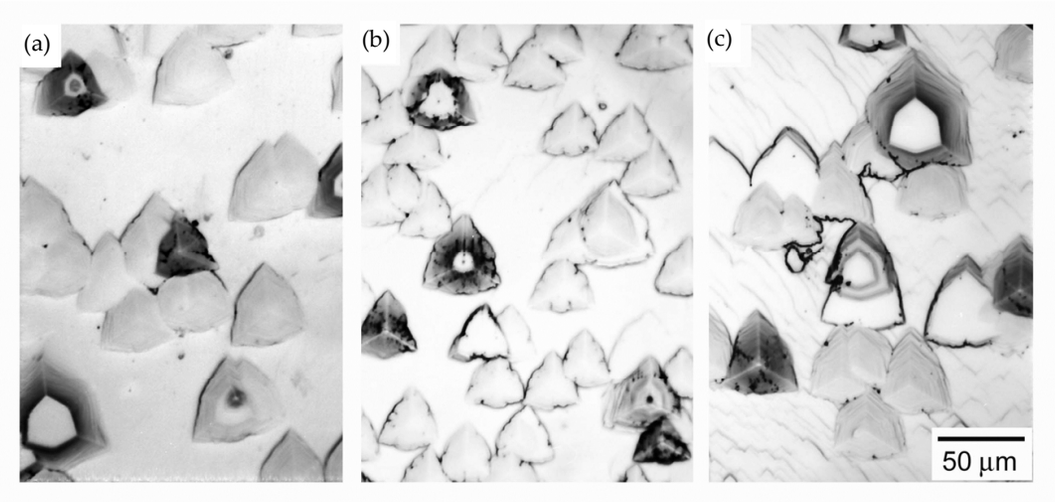

Figure 4. Optical micrographs of the surface that were anodically dissolved under potentiostatic electrolysis at higher overpotentials of (a): 156 mV; (b): 166 mV; (c): 176 mV.

2.4. Measurement of anodic current density

2.4.1. Steady anodic current densities at lower overpotentials

The initial steep decrease of current density is principally due to the fact that a diffusion layer of the dissolved atoms (ions) forms in the neighborhood of crystal surface in process of time so as to decrease the undersaturation which is driving force for the dissolution. Therefore an approximately constant current density after its initial steep decrease is thought to be a steady current density i_s which flows accompanying with the consecutive two dissolution processes consisting of surface reaction and volume diffusion of dissolved atoms. This shows that the copper crystal/electrolyte system is a quasi-reversible electrode. Also the steady anodic current densities at lower overpotentials are thought to have only a little influence of formation of dislocation etch pits. Thus we assume that i_s is related to the vertical dissolution rate v_s at dislocation-free site of surface, which is given by the following expression (Schaarwächter and Lücke, 1967):

$$v_s = \frac{\Omega}{ne} i_s \tag{1}$$

where e [C] is elementary charge (electronic charge), n [1] the charge number transferred at reaction and Ω [m^3] the atomic volume.

In this experiment, the potentiostatic electrolysis at overpotentials in a range from about 60 mV to 125 mV were carried out for 600 s at each temperature of 268, 283, 298 and 308 K and the relationships between the steady anodic current densities i_s and applied overpotentials η were investigated.

2.4.2. Minimum anodic current densities at higher overpotentials

On the other hand, the current density reaches a minimum after an initial steep decrease as shown in the curve of 176 mV in Fig.2 when an overpotential higher than about 125mV was applied. Then it tends to increase gradually together with fluctuating and take a higher steady value as described in Section 2.3. This is thought to be due to the fact that etch pits remarkably formed at dislocation sites and grew along with time under higher overpotential as shown in Fig.4 (Schaarwächter and Lücke, 1967; Imashimizu and Watanabé, 1983). That is, it is because nucleation and growth of etch pits at dislocation site resulted in an increase of the anodic current density which represents an average dissolution rate of whole surface exposed to electrolyte solution as the areas occupied by etch pits increase. Based on the above knowledge, we assume that the initial minimum current density i_{sm} under potentiostatic electrolysis at higher overpotentials is approximately equal to a current density that is equivalent to the dissolution rate of dislocation-free site of surface because the contribution to anodic current density of dislocation etch pit formation is thought to be a little in the initial stage of electrolysis. That is, an average value of i_{sm} was assumed to give the vertical dissolution rate at dislocation-free site of surface approximately as represented by the relation:

$$v_s \approx v_{sm} = \frac{\Omega}{ne} i_{sm} \tag{2}$$

Thus the electrolysis experiment was carried out for a prescribed time from 60 s to 360 s at each overpotential of 156, 166, 176 and 186 mV keeping the temperature at 298 K and at each temperature of 268, 283, 298 and 308 K under an overpotential of 176 mV. The initial minimum current densities i_{sm} were obtained from the anodic current density/time curves measured under every condition.

2.5. Measurement of polarization curve and estimation of the diffusion-limited current densities

It needs to estimate activation overpotential η_a and concentration overpotential η_c for analyzing the relationship between anodic current density and applied overpotential as described in Section 1. Thus the polarization curves in a range of overpotential of about -400 mV to 400 mV were measured three times at each temperature of 298K and 308K by the potential step method. Then the anodic and cathodic diffusion-limited current densities were estimated.

2.6. Direct measurement of dissolution rates of surface

2.6.1. Vertical dissolution rate of surface

After the (111) surface of a copper crystal specimen was anodically dissolved at every condition of specified overpotrntials and temperatures as described in Section 2.4.2, it was

observed by use of the optical microscope equipped with objective lenses for two-beam interferometry and multiple interferometry.

Figure 5 (a) shows the micrograph of a part of boundary region between the crystal surface exposed to the electrolyte solution and the peripheral portion covered with vinyl seal, which was photographed with two-beam interferometry mode. The vertical dissolution amounts s of surface shown by the illustration was measured from a deviation of the interference stripes caused by the step which was formed at that boundary region after dissolved. The vertical dissolution amounts s of surface under each condition was plotted against dissolution time t. The increasing rate $\dot{s}$ of s with t was obtained from the gradient of each linear relationship, and the vertical dissolution rate of surface under every condition was estimated by the $\dot{s}$.

2.6.2. Dissolution rates at dislocation site of surface

Figures 5 (b) and (c) show a pair of micrographs of identical dislocation etch pits formed on dissolved surface which were photographed with optical mode and multiple interferometry mode. In this work, the depth d of the dark (deep) pits that were formed at positive edge dislocation sites (see Appendix A1) were measured by drawing the vertical cross sections of the pits that is shown by the illustration with use of the micrograph pairs such as Figs.5 (b) and (c). Also the width w (average distance from center to the three sides of pit) of those dark pits that is shown by the illustration were measured on the micrograph such as Fig.5 (b). Measurements of the depth and width of pit were performed about more than 20 dark pits formed on the surface dissolved under every condition, and the respective average values d and w were obtained. The depth d and the width w of dark pits were plotted against dissolution time t.

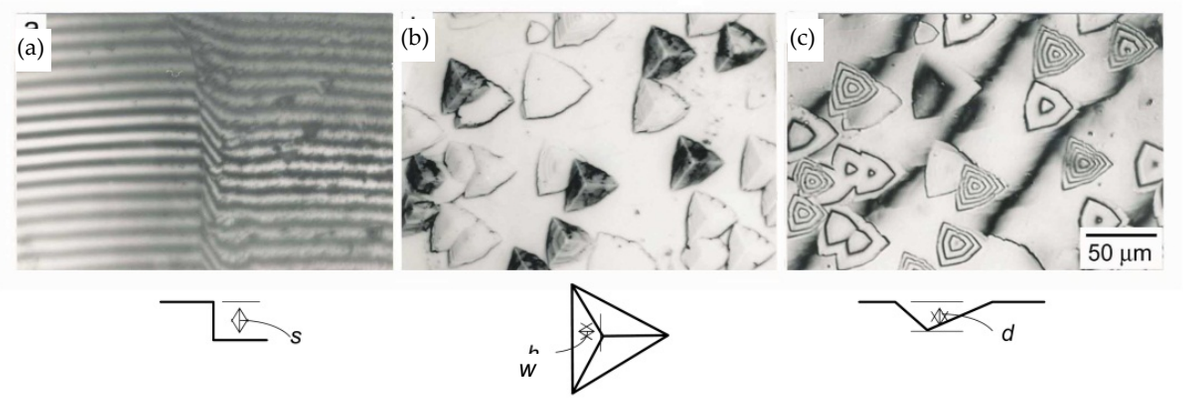

Figure 5. (a): Two-beam interferometry micrograph at the boundary between dissolved and undissolved surfaces; (b): Optical micrograph; (c): Multiple interferometry micrograph of the same view as b.

The increasing rate $\dot{d}$ of d with t was obtained from the gradient of each linear relationship, and the vertical dissolution rate v_{ed} at edge dislocation site was estimated by

$$v_{ed} = \dot{d} + v_s, \tag{3}$$

where v_s means the vertical dissolution rate at dislocation-free site of the surface. Also the increasing rate $\dot{w}$ of w with t was obtained from the gradient of each linear relationship, and the lateral dissolution rate v_w at edge dislocation site was estimated from the relation:

$$v_{\mathrm{w}} = \frac{w}{d} v_{\mathrm{ed}} \approx \frac{\dot{w}}{\dot{d}} \left(\dot{d} + v_{\mathrm{s}} \right). \tag{4}$$

2.7. Analysis of relationship between current density and overpotential

Under potentiostatic electrolysis of the copper/electrolyte system in the present experiment, the copper crystal is thought to be dissolved accompanying an anodic current according to a simple electrode reaction expressed by the following equation (Lal and Thirsk, 1953; Jasper and Scaarwächter, 1966):

$$\mathrm{Cu} + 2\mathrm{Cl}^- \rightarrow \mathrm{CuCl}_2^- + \mathrm{e}, \tag{5}$$

where the contribution to current density of reaction of Br^- ion involved in dissolution process as inhibitor is assumed to be disregarded. The anodic current density i_s flowing steadily at an applied overpotential η is generally expressed by a relation:

$$i_{\mathrm{s}} = i_0 \left\{ \left(\frac{C_{\mathrm{Cl}^-}}{C^0_{\mathrm{Cl}^-}} \right)^2 \exp\left(\frac{\alpha n e \eta}{kT} \right) - \frac{C_{\mathrm{CuCl}_2^-}}{C^0_{\mathrm{CuCl}_2^-}} \exp\left(-\frac{(1-\alpha) n e \eta}{kT} \right) \right\}, \tag{6}$$

where exchange current density i_0 is represented by

$$i_0 = n e \beta k_{\mathrm{s}} C^{0\,2(1-\alpha)}_{\mathrm{Cl}^-} C^{0\,\alpha}_{\mathrm{CuCl}_2^-} \nu \exp\left(-\frac{\Delta H_0}{kT} \right) \tag{7}$$

(Tamamushi, 1967; Maeda 1961). k_s is surface density of kink that is active site at dissolution of surface atom, α the transfer coefficient, ΔH_0 the activation energy (enthalpy) at dissolution of an atom, ν the atomic frequency, and β a supplementary factor of rate constant of electrode reaction. Also, C_{Cl^-} and $C_{CuCl_2^-}$ are the surface concentrations of Cl^- and $CuCl_2^-$ ions involved in a steady anodic dissolution, and $C^0_{Cl^-}$ and $C^0_{CuCl_2^-}$ the ones in equilibrium state. They are represented as a relative surface density as follows.

If the electrolyte solution contacting with crystal surface contained X ions of m kmol m^{-3}, the surface concentration C_X [1] can be expressed by the following relation:

$$C_{\mathrm{X}} = \frac{m \times 10^3 N_{\mathrm{A}} \left[\mathrm{m}^{-3} \right] \times \xi \left[\mathrm{m} \right]}{\left(bb^* \right)^{-1} \left[\mathrm{m}^{-2} \right]}, \tag{8}$$

where N_A is the Avogadro constant, bb^* the area occupied by an atom and ξ the thickness of electrolyte solution layer contacting with the crystal surface (Imashimizu, 2011).

The anodic dissolution of copper crystal in this experiment is thought to proceed quasi-reversibly with a surface reaction and volume diffusion of dissolution atom as described in Section 2.4.1. So we assume that the activation overpotential η_a and the concentration overpotential η_c are written by

$$\eta_a = \eta - \eta_c \quad \text{and} \quad \eta_c = \frac{kT}{ne}\ln\left\{\frac{C_{CuCl_2^-}/C^0_{CuCl_2^-}}{\left(C_{Cl^-}/C^0_{Cl^-}\right)^2}\right\}, \tag{9}$$

where the folloing relations:

$$\frac{C_{Cl^-}}{C^0_{Cl^-}} = 1 - \frac{i_s}{i_{lCl^-}}, \quad \frac{C_{CuCl_2^-}}{C^0_{CuCl_2^-}} = 1 - \frac{i_s}{i_{lCuCl_2^-}} \tag{10}$$

are given, if i_{lCl^-} and i_{lCuCl2^-} are the anodic and cathodic diffusion-limited current densities of the electrode reaction respectively (Tamamushi, 1967). Thus activation overpotential η_a and concentration overpotential η_c are assumed to be given by Eqs.(9) and (10), when the anodic dissolution of copper crystal proceeds steadily at an applied overpotential η by a quasi-reversible electrode reaction of Eq.(5). Also surface undersaturation σ is defined by

$$\sigma = 1 - \exp\left(-\frac{ne\eta_a}{kT}\right) = 1 - \exp\left(-\frac{ne\eta}{kT}\right)\left\{\frac{C_{CuCl_2^-}/C^0_{CuCl2^-}}{\left(C_{Cl^-}/C^0_{Cl^-}\right)^2}\right\}. \tag{11}$$

Then, the Eq.(6) is reduced to

$$i_s = ne\beta k_s C^{0\,2(1-\alpha)}_{Cl^-} C^{0\,\alpha}_{CuCl_2^-}\left(\frac{C_{Cl^-}}{C^0_{Cl^-}}\right)^2 \sigma\nu\exp\left(-\frac{\Delta H_0 - \alpha ne\eta}{kT}\right) \tag{12}$$

by using Eqs. (7), (9) and (11). Also Eq.(12) leads to the following relation:

$$i_s\left(\frac{C_{Cl^-}}{C^0_{Cl^-}}\right)^{-2}\sigma^{-1} = i_0(T)\exp\left(\frac{\alpha ne\eta}{kT}\right). \tag{13}$$

Thus if the anodic and cathodic diffusion-limited current densities i_{lCl^-} and i_{lCuCl2^-} are obtained, the experimental relationship of i_s/η would be represented with use of Eqs.(10) and (11) by Eq.(13). Then α and $i_0(T)$ would be estimated from the gradient and the constant term of the linear relationship of $\ln\{i_s(C_{Cl^-}/C^0_{Cl^-})^{-2}\sigma^{-1}\}$ vs. $ne\eta/kT$. Also ΔH_0 would be estimated from the gradient of the linear relationship of $\ln\{i_0(T)\}$ vs. $1/T$.

On the other hand, concerning the complex term consisting of surface concentrations of Cl^- and $CuCl_2^-$ ions,

$$C_{\mathrm{Cl}^-}{}^{2(1-\alpha)} C_{\mathrm{CuCl_2}^-}{}^{\alpha} = C^0{}_{\mathrm{Cl}^-}{}^{2(1-\alpha)} C^0{}_{\mathrm{CuCl_2}^-}{}^{\alpha} \left(\frac{C_{\mathrm{Cl}^-}}{C^0{}_{\mathrm{Cl}^-}} \right)^2 \exp\left(\frac{\alpha n e \eta_c}{kT} \right) \tag{14}$$

is lead from Eq.(9). Therefore applying Eq.(14) to Eq.(12) lead to

$$i_s = ne\beta k_s C_{\mathrm{Cl}^-}{}^{2(1-\alpha)} C_{\mathrm{CuCl_2}^-}{}^{\alpha} \sigma \nu \exp\left(-\frac{\Delta H}{kT} \right), \tag{15}$$

where ΔH is given by the relation:

$$\Delta H = \Delta H_0 - \alpha n e \eta_a . \tag{16}$$

We can see that Eqs.(15) and (16) are formulae for the steady current density expressed with use of the parameters β, k_s, C_{Cl^-}, C_{CuCl2^-}, σ, α and ΔH involved in the surface reaction process when the anodic dissolution progresses steadily by a quasi-reversible electrode reaction.

Thus undersaturation σ, transfer coefficient α and activation enthalpy ΔH_0 for the anodic dissolution reaction of copper crystal/electrolyte system will be estimated from experimental results, and a supplementary factor β and kink density k_s will be examined by a model of crystal dissolution in this study.

3. Experimental results

3.1. Polarization curves and undersaturation in anodic dissolution

The polarization characteristic of the copper crystal/electrolyte system at 298K is shown in Fig. 6. The anodic and cathodic diffusion-limited current densities i_{Cl^-} and i_{CuCl2^-} shown in the diagram were obtained by averaging the values measured three times. Table 1 shows those diffusion-limited current densities obtained from the polarization characteristics measured at 298 and 308 K by a similar method.

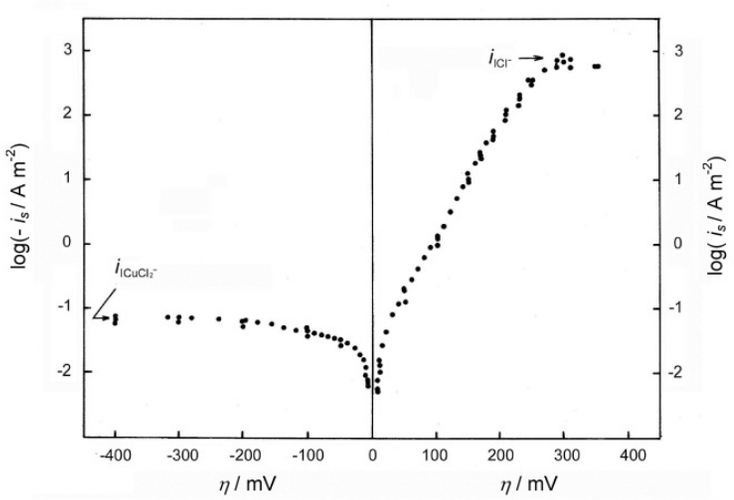

Figure 6. Polarization curve of the copper crystal/elecrolyte system. i_{Cl^-} and i_{CuCl2^-} mean the anodic and cathodic difffusion-limited current densities.

T /K	i_{ICl^-}/A m^{-2}	$i_{ICuCl_2^-}$/ A m^{-2}
298	827	-0.0732
308	1072	-0.156

Table 1. Measurements of the anodic and cathodic diffusion-limited current densities i_{ICl^-} and $i_{ICuCl_2^-}$.

The undersaturation σ were estimated from experimental polarization characteristics such as Fig.6 with use of Eqs.(10) and (11). The diagram that plotted σ against $ne\eta/kT$ in a range of ($ne\eta/kT$) about 0 to 6 is shown in Fig.7. The black dots in the diagram show the values of σ which are calculated from the (i_s/i_{ICl^-})/($ne\eta/kT$) relationship that was derived by substituting the experimental values i_0, α, i_{ICl} and i_{ICuCl_2} into Eq.(6).

The experimental relationships of σ/($ne\eta/kT$) at 298K and 308K approximately consist with each other, and also with the calculated relationship. However, the experimental curves of σ/($ne\eta/kT$) deviate from the calculated curve in a range of ($ne\eta/kT$) larger than about 5. This is because the experimental current density includes an increase of current density attributed to significant formation of etch pits at higher overpotentials than about 125 mV. We assumed that the σ/($ne\eta/kT$) relationship does not almost depend on temperature from the result of Fig.7.

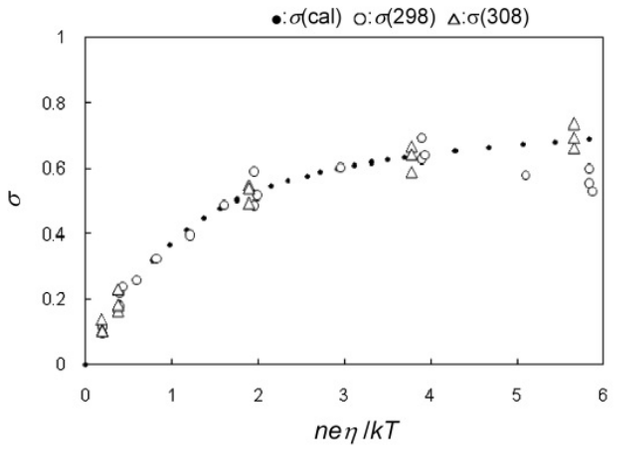

Figure 7. Plots of undersaturation σ against normalized overpotential $ne\eta/kT$. σ(298) and σ(308) designate experimental values at 298K and 308K respectively. σ(cal) is the calculated one.

3.2. Estimations of parameters controlling exchange current density

Figure 8 is the diagram that plotted the steady current densities against overpotentials lower than 127 mV which were measured at 268K, 283K, 298K and 308K. Figure 9(a) is the diagram that plotted $\ln(i_s\sigma^{-1})$ obtained from Fig. 8 against $ne\eta/kT$ at every temperature taking account of $(C_{Cl^-}/C^0_{Cl^-})^{-2} \approx 1$. The linear relationships at every temperature in the diagram are drawn so that they have a same gradient given by averaging. The transfer coefficient α was estimated from the gradient of their linear relationships. Then also the exchange current densities $i_0(T)$ at each temperature were estimated from the constant terms of them. Figure 9(b) is the diagram that plotted $\ln\{i_0(T)\}$ against $1/T$. The activation enthalpy for the anodic dissolution reaction of copper crystals was estimated from the gradient of the linear relationship shown in Fig. 9(b).

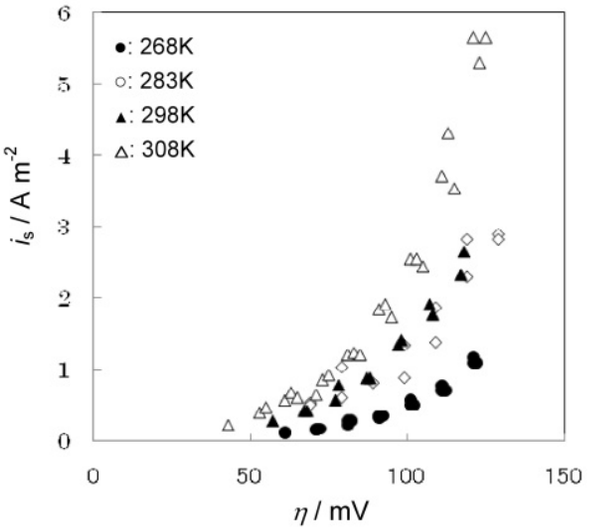

Figure 8. Plots of steady current densities against overpotentials lower than about 125 mV

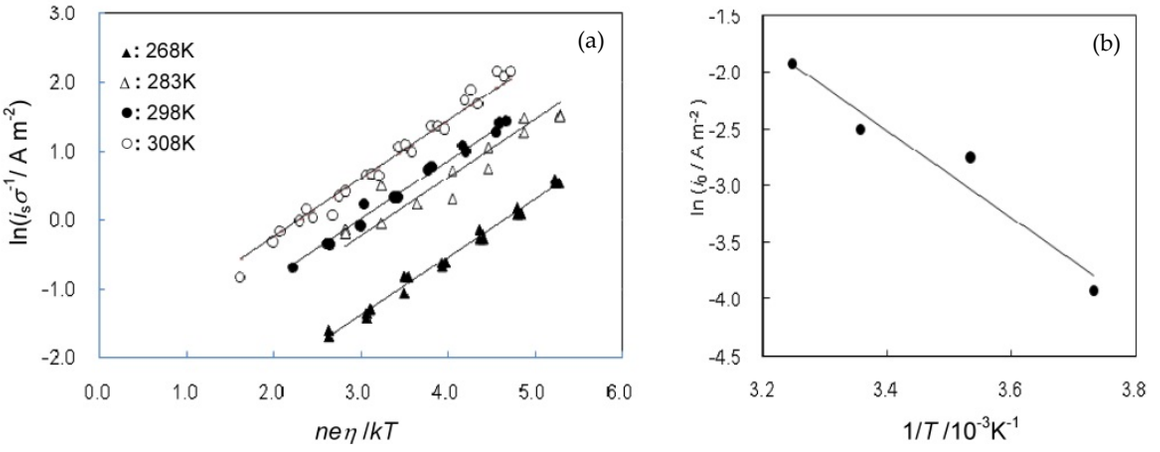

Figure 9. (a): Plots of $\ln(i_s\sigma^{-1})$ against $ne\eta/kT$; (b): Plot of $\ln\{i_0(T)\}$ against $1/T$.

Then, because surface concentrations C^0_{Cl}-and C^0_{CuCl2} of Cl^- and $CuCl_2^-$ ions are calculated by Eq.(8) when (111) surface of a copper crystal is in equilibrium with the electrolyte solution consisting of 5 kmol m^{-3} NaCl and 10^{-4} kmol m^{-3} CuCl, the complex term $C^0_{Cl}{}^{-2(1-\alpha)}C^0_{CuCl2}{}^{-\alpha}$ in Eq.(7) giving exchange current density can be evaluated by using the transfer coefficient α estimated above.

Thus the estimations of parameters controlling exchange current density are summarized in Table 2. The value of βk_s was evaluated by substituting i_0, ΔH_0 and $C^0_{Cl}{}^{-2(1-\alpha)}C^0_{CuCl2}{}^{-\alpha}$ into Eq.(7), where the atomic frequency $\nu = 6.21\times10^{12}$ [s^{-1}], elementary electric charge, $e = 1.602\times10^{-19}$[C] and $n = 1$ were assumed.

α	ΔH_0 / eV	i_0 /10^{-2}A m^{-2}	$C^0_{Cl}{}^{-2(1-\alpha)}C^0_{CuCl2}{}^{-\alpha}$	βk_s /10^{16} m^{-2}
0.84	0.33	8.2*	2.36×10^{-6}	1.32

* the value at 298K

Table 2. Estimation of transfer coefficient α, activation enthalpy ΔH_0, exchange current density i_0 at 298K, and a factor βk_s affecting reaction rate constant.

3.3. Anodic dissolution rates at higher overpotentials

3.3.1. Estimation of vertical dissolution rate of surface from anodic current density

Figures 10 (a) and (b) are examples of the anodic current density/time curves which were recorded when the copper crystal was dissolved for 240 s at higher overpotential. The vertical dissolution rate v_{sm} at dislocation-free site of surface under every condition was determined from an average of the initial minimum current densities i_{sm} pointed by arrow of i/t curves (measured for five different dissolution time in a range of 60 s to 360 s under each condition) shown in Fig.10 as described in Sections 2.4.2.

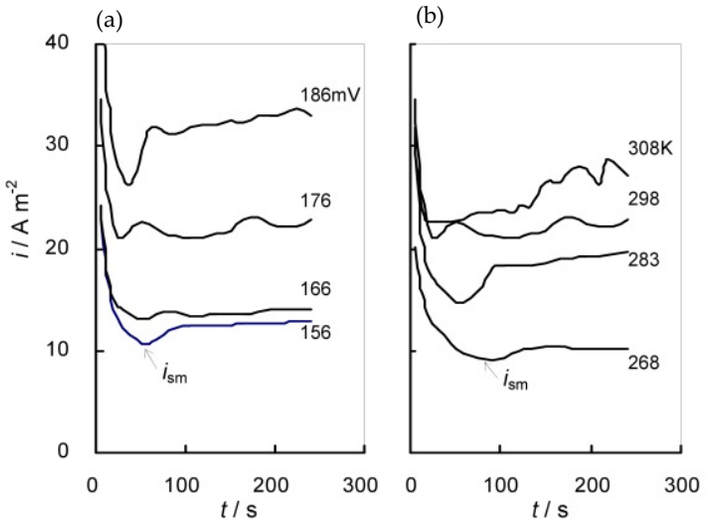

Figure 10. Examples of anodic current density/time curves. (a): The effect of overpotential; (b): The effect of temperature. Initial minimum i_{sm} was obtained in every curve.

3.3.2. Estimation of vertical dissolution rate of surface by direct measurement

Figures 11 (a) and (b) are the diagrams that plotted vertical dissolution amounts s of surface against dissolution time t as described in Sections 2.6.1. The vertical dissolution rates $\dot{s}$ of surface were estimated from the gradient of the linear relationship of s/t shown in Fig.11.

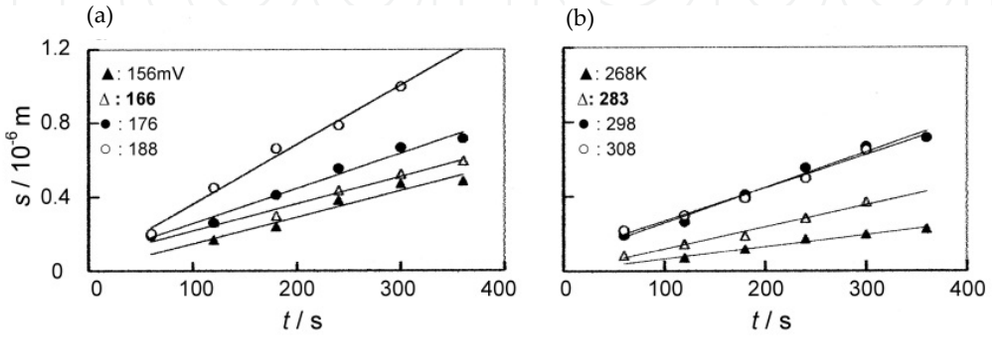

Figure 11. Vertical dissolution amounts of surface vs. dissolution time. (a): Effect of overpotential at 298K; (b): Effect of temperature at 176mV

3.3.3. Estimation of dissolution rates at edge dislocation site by direct measurement

Figures 12 (a) and (b) are the diagram that plotted the depth d of the dark etch pits which were formed at positive edge dislocation sites on the surface dissolved under each condition against dissolution time t, as described in Sections 2.6.2. Also Figs.13 (a) and (b) are the diagrams that plotted similarly the width w of the same dark etch pits as the above mention against dissolution time t. The increasing rate $\dot{d}$ of depth d of etch pit with t and the increasing rate $\dot{w}$ of width w with t were obtained from the gradient of each linear relationship shown in those results.

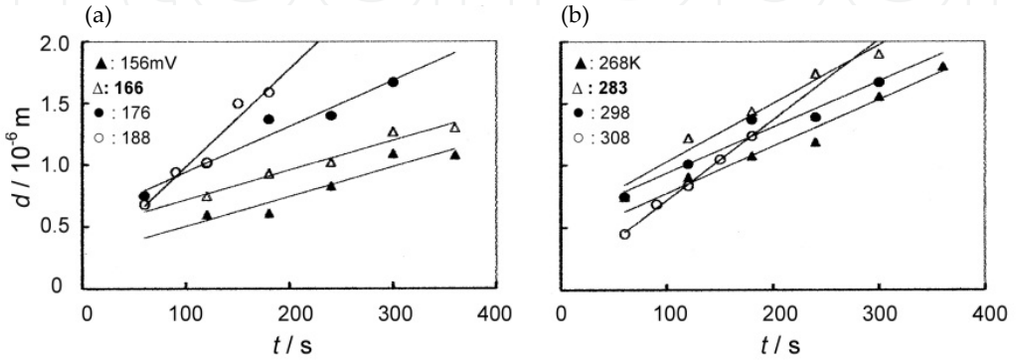

Figure 12. Depth of dark etch pit vs. dissolution time. (a): Effect of overpotential at 298K; (b): Effect of temperature at 176mV

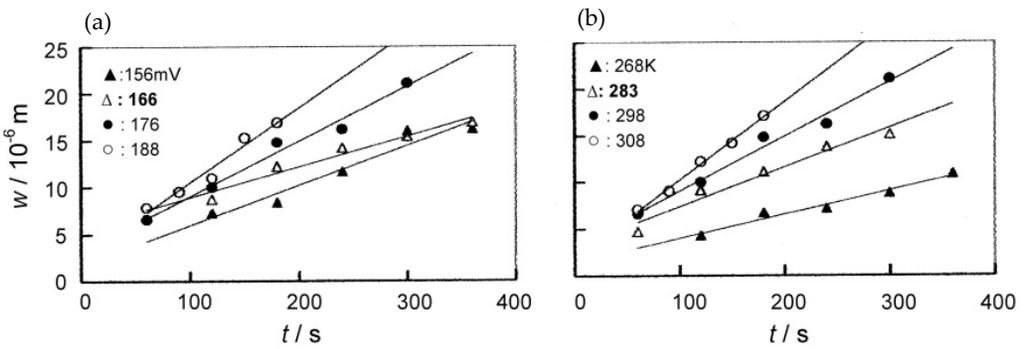

Figure 13. Width of dark etch pit vs. dissolution time. (a): Effect of overpotential at 298K; (b): Effect of temperature at 176mV.

3.4. Effects on the dissolution rates of overpotential and temperature

Figures 14 (a) and (b) are the diagrams that plotted the logarithm values of the dissolution rates. It can be seen that the value of log v_{sm} approximately consists with that of log $\dot{s}$. This shows that both v_{sm} and $\dot{s}$ represent the dissolution rate v_s of dislocation-free site of surface approximately. However, the value of v_{sm} seems to be more exact than that of $\dot{s}$, because while the former is a quantity related to total dissolution amounts of whole surface, the latter is that related to the dissolved amounts of a part of surface near to boundary between the portion exposed to electrolyte solution and the portion covered by vinyl seal. Thus the dissolution rate v_s of dislocation-free surface was assumed to be given not by $\dot{s}$ but v_{sm}. Then v_{ed} and v_w in Fig.14 show the values estimated from Eq.(3) and Eq.(4) in which v_s was substituted by v_{sm}.

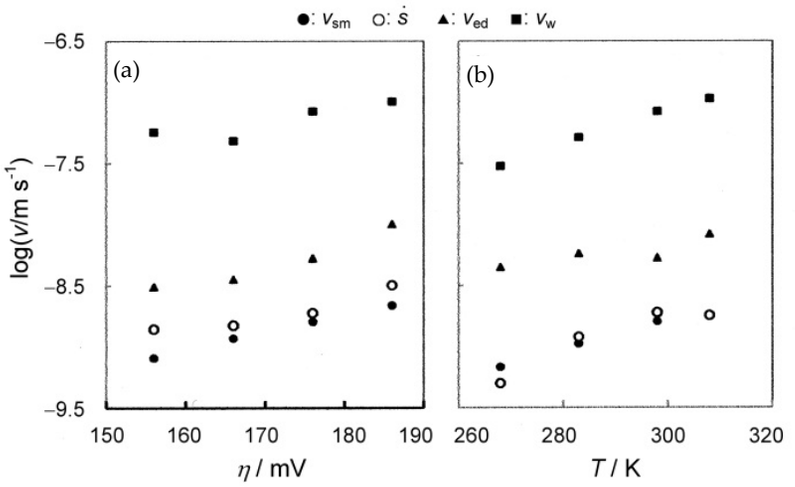

Figure 14. (a): Plots on a logarithmic scale of dissolution rates v_{sm}, $\dot{s}$, v_{ed}, and v_w against overpotential η; (b): Similar plots of v_{sm}, $\dot{s}$, v_{ed}, and v_w against temperature T

It can be seen that both log v_{sm} and log v_w tend to increase rather homogeneously with an increase of η, from Fig.14 (a). However, the tendency of log v_{ed} are somewhat different and in accelerative. Also, it can be seen from Fig.14 (b) that though log v_{sm} and log v_w tend to similarly increase with an increase of T, the tendency of log v_{ed} are somewhat little, compared to the former two. This is seen from the fact that the increasing rate ($\Delta\log v_{ed}/\Delta T = 5.4\times10^{-3}$) of the latter is less than that ($\Delta\log v_{sm}/\Delta T = 1.1\times10^{-2}$, $\Delta\log v_w/\Delta T = 1.4\times10^{-2}$) of the former two.

4. Discussion

4.1. Atomistic dissolution model of crystal surface

4.1.1. Vertical dissolution rate at dislocation-free site of surface

Concerning the dissolution of a crystal, the atomistic model illustrated in schematic diagram of Fig.15 has been proposed (Burton et al., 1951; Schaarwächter, 1965). The dissolution of crystals proceeds via a lateral retreat motion of surface step of an atomic height that is induced by dissolving of surface atom from the kink sites into the solution. The vertical dissolution rate v_s of surface is given by lateral retreat rate v_h and surface density $\tan\theta$ of surface step, which is expressed by the following equation:

$$v_s = v_h \tan\theta = v_h \frac{a}{\lambda}, \tag{17}$$

where θ is an average inclination of crystal surface to a low index face, a an atomic height of surface step, and λ the mean distance between adjacent surface steps. The lateral retreat rate v_h of surface step is expressed by

$$v_h = b^* k^* \sigma_s \nu \exp\left(-\frac{\Delta H_s}{kT}\right), \tag{18}$$

where ΔH_s is the activation enthalpy for dissolution of an atom at kink site of surface step, ν the atomic frequency, k^* the retreat rate constant of surface step, and b^* the unit retreat distance. σ_s is surface undersaturation, which is written as

$$\sigma_s = 1 - \exp\left(-\frac{\Delta\mu}{kT}\right), \tag{19}$$

where $\Delta\mu$ is the chemical potential difference of dissolution atom between two phases of a crystal/ solution system (Schaarwächter, 1965).

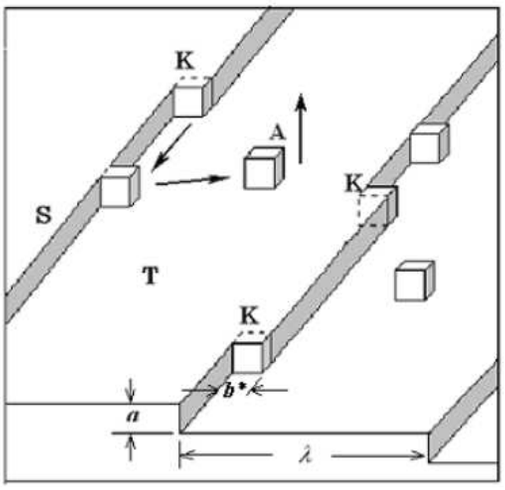

Figure 15. Atomistic model for dissolution process of a crystal surface. Atom dissolves from kink site of surface step into solution. K: Kink; S: Surface step; T: Terrace; A: Ad-atom

4.1.2. Lateral dissolution rate at edge dislocation site

The dislocation etch pit is thought to be formed via a successive nucleation and growth processes of two-dimensional pits at the dislocation site (Schaarwächter, 1965) or via a spiral dissolution of the surface step which is caused by screw dislocation (Cabrera and Levine, 1956). We discuss the dissolution rate at edge dislocation site of (111) surface of copper crystals, based on a nucleation and growth model of two-dimensional pits (Schaarwächter, 1965) that is illustrated in Fig 16, in the following.

Since the lateral dissolution rate v_w is thought to represent horizontal growth rate of two-dimensional pit nucleated at edge dislocation site of surface, it may be corresponding to the lateral retreat rate v_h of surface step along (111) face. Thus we assume that v_h is given by v_w as shown in the following relation:

$$v_h \approx v_w. \tag{20}$$

4.1.3. Vertical dissolution rate at edge dislocation site

On the other hand the vertical dissolution rate at positive edge dislocation site would be examined by the nucleation rate of two-dimensional pit at dislocation site as follows.

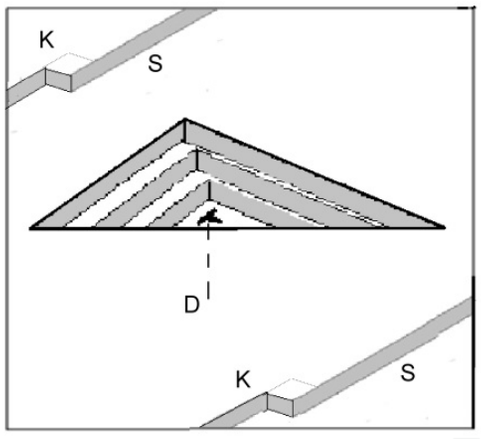

Figure 16. Illustration for dislocation etch pit formation by successive nucleation and growth of two-dimensional pits. D: Dislocation; S: Surface step; K: Kink.

According to the classical nucleation theory, if ΔG_{ed}^* is the critical free energy change at nucleation of a two-dimensional pit at edge dislocation site, a steady state nucleation rate I of two-dimensional pit would be expressed by

$$I = Zr\exp\left(-\frac{\Delta G_{ed}^*}{kT}\right), \tag{21}$$

where r is a separation rate of an atom from an active site of the two-dimensional pit into the solution and Z the Zeldovich factor (Toschev, 1973). Since the separation rate r is assumed to be a similar quantity to the dissolution rate of an atom from kink site of surface, it depends on the surface concentrations of Cl^- and $CuCl_2^-$ ions as known from the Eq. (15) in Section 2.7, and is expressed by

$$r \propto C_{Cl^-}^{2(1-\alpha)} C_{CuCl_2^-}^{\alpha} \nu \exp\left(-\frac{\Delta H_0}{kT}\right). \tag{22}$$

Accordingly, the vertical dissolution rate v_{ed} at edge dislocation site of surface is expressed by

$$v_{ed} = aK_s C_{Cl^-}^{2(1-\alpha)} C_{CuCl_2^-}^{\alpha} \nu \exp\left(-\frac{\Delta G_{ed}^* + \Delta H}{kT}\right), \tag{23}$$

where a is the depth of "two-dimensional pit and K_s is an undetermined constant including Zeldovich factor and others (see Appendix A2.).

According to the nucleation theory of dissolution of crystals, ΔG_{ed}^* is small compared to ΔG_s^* which is the critical free energy change at nucleation of a two-dimensional pit at dislocation-free site of surface, because of strain energy of dislocation core. It is expressed by

$$\Delta G_{ed}^* = p\Delta G_s^* = p\frac{\pi a \Omega \gamma^2}{\Delta \mu} \tag{24}$$

and

$$p = \left(1 - \frac{\alpha_C q}{4\pi}\frac{Gb}{\gamma}\right)^2 \leq 1, \tag{25}$$

where γ is the interfacial free energy of the crystal and solution at step of the two-dimensional pit, G the shear modulus and q and α_c the constants (Schaarwächter, 1965).

4.2. Relations between vertical dissolution rate of surface and anodic current density

4.2.1. Expression for dissolution rate of dislocation-free site of surface

When the copper crystal is anodically dissolved by the simple electrode reaction of Eq.(5) the vertical dissolution rate v_s of dislocation-free surface at lower overpotentials and the v_{sm} at higher overpotentials would be estimated by Eq.(1) and Eq.(2) respectively as described in Section 2.4. Thus it is experimentally estimated with use of Eqs. (1), (2), and (15) by the following expression:

$$v_{sm} \approx v_s = \Omega\beta k_s C_{Cl^-}{}^{2(1-\alpha)} C_{CuCl_2^-}{}^{\alpha} \sigma\nu \exp\left(-\frac{\Delta H}{kT}\right). \tag{26}$$

According to the dissolution model of crystals, the dissolution rate at dislocation-free site of surface is expressed from Eqs. (17) and (18) by

$$v_s = \frac{a}{\lambda} b^* k^* \sigma_s \nu \exp\left(-\frac{\Delta H_s}{kT}\right). \tag{27}$$

Therefore, the following relations are obtained from Eqs.(16), (26) and (27) concerning the rate constant of the lateral retreat rate of surface step and activation enthalpy for the dissolution.

$$k^* = \beta\frac{b}{x_0} C_{Cl^-}{}^{2(1-\alpha)} C_{CuCl_2^-}{}^{\alpha} = \beta\frac{b}{x_0} C^0{}_{Cl^-}{}^{2(1-\alpha)} C^0{}_{CuCl_2^-}{}^{\alpha} \left(\frac{C_{Cl^-}}{C^0{}_{Cl^-}}\right)^2 \exp\left(\frac{\alpha ne\eta_c}{kT}\right) \tag{28}$$

and

$$\Delta H_s = \Delta H = \Delta H_0 - \alpha ne\eta_a \tag{29}$$

Also from Eqs. (11) and (19)

$$\Delta\mu = ne\eta_a \tag{30}$$

is obtained. It can be seen that the rate constant k^* of lateral retreat motion of surface step is electrochemically expressed by Eq.(28) and that it increases with an increase of concentration overpotential η_c.

4.2.2. Estimation of kinetics parameters controlling the dissolution rate

As mentioned above the dissolution rate v_{sm} at dislocation-free site of surface under higher overpotentials is expressed by an approximate equation:

$$v_{sm} \approx \Omega\beta k_s {C^0}_{Cl^-}{}^{2(1-\alpha)} {C^0}_{CuCl_2^-}{}^{\alpha} \sigma\nu \exp\left(-\frac{\Delta H_0 - \alpha ne\eta}{kT}\right), \tag{31}$$

from Eqs. (14) and (26), where we assumed $i_s << i_{lCl^-}$, that is,

$$\frac{C_{Cl^-}}{C^0_{Cl^-}} = 1 - \frac{i_s}{i_{lCl^-}} \approx 1. \tag{32}$$

Thus concerning the dissolution rate at dislocation-free site of surface which have a constant kink density k_s, a following approximate expression is lead from Eq.(31) (Imashimizu, 2011).

$$\ln v_{sm} \approx \ln(\nu\ \Omega\beta k_s {C^0}_{Cl^-}{}^{2(1-\alpha)} {C^0}_{CuCl_2^-}{}^{\alpha}) + \ln(\sigma) - \frac{\Delta H_0 - \alpha ne\eta}{kT} \tag{33}$$

Figures 17 (a) and (b) are the diagrams that plotted the dissolution rate v_{sm} shown in Figs.14 (a) and (b) on a natural logarithmic scale against η (T = 298K) and $1/T$ (η =176mV) respectively. It can be seen that the values of ($\alpha ne/kT$) and (($\Delta H_0 - \alpha ne\eta$)/$k$) are estimated by comparing the Eq.(33) with gradients of the linear relationships drawn in Figs. 17 (a) and (b), because the overpotential and temperature dependences of σ in the range of 156 mV to 186 mV are assumed to be a little. Thus, α and ΔH_0 were also obtained from overpotential dependence of vertical dissolution rate v_{sm} of surface at higher overpotentials and temperature dependence of that. The estimations are shown in Table 3, showing α and ΔH_0 are in good agreement with those values in Table 2.

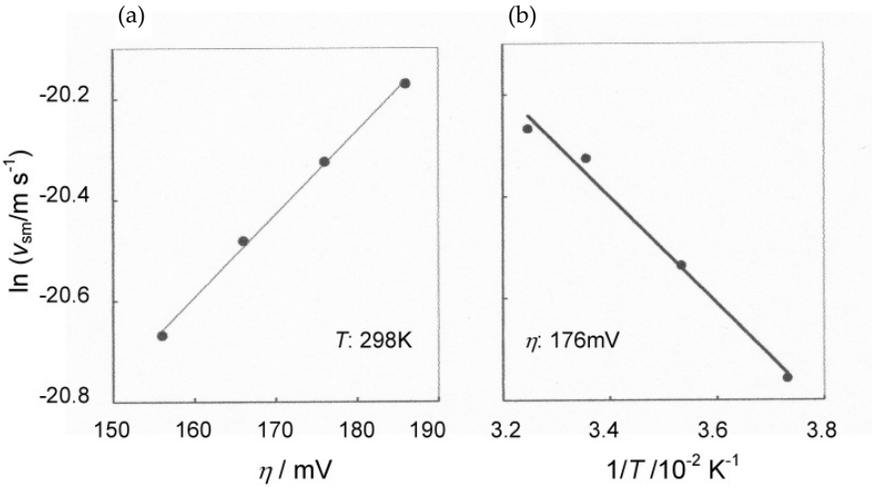

Figure 17. Vertical dissolution rate v_{sm} at dislocation-free site of surface on a natural logarithm scale. (a): The plot against overpotential η; (b): The plots against the inverse $1/T$ of temperature.

According to atomistic dissolution model of a crystal surface illustrated in Fig.15, the relation of $\theta = \tan^{-1}(a/\lambda) = \tan^{-1}(v_s/v_h)$ is lead from Eq. (17), which represents the inclination angle of surface to (111) face. Since it is approximately given by $\theta \approx \theta^* = \tan^{-1}(v_{sm}/v_w)$ with use of Eqs.(20) and (26), the values of θ^* obtained from Fig.14 were plotted against η and T in Figs.18 (a) and (b). It can be seen that the tendencies of change in θ^* against η and T are not clear and not reasonable. The average value of θ^*_{av} is 2.1×10^{-2} rad, which is a little large compared to a deviation 8.7×10^{-3} rad from [111] direction that was aimed when we prepared the surface of specimen as described in Section 2.1. This is probably attributed to the fact that actual surface exposed to electrolyte solution was slightly spherical as a whole and was having microscopic swells. That is, the variation of their values seems to be due to experimental error. Thus the vertical dissolution rate at dislocation-free site of surface is assumed to be given by retreat rate of the surface steps which preexists on the prepared surface, which gives following relation:

$$\beta k_s = \beta \frac{1}{\lambda x_0} \approx \beta \frac{b}{x_0} \frac{\tan\theta^*}{ab} \tag{34}$$

Accordingly $\beta(b/x_0)$ is calculated from βk_s in Table 2 by using Eq. (34), which is shown in Table 3 where assumed $\theta^* = \theta^*_{av}$ (0.021 rad).

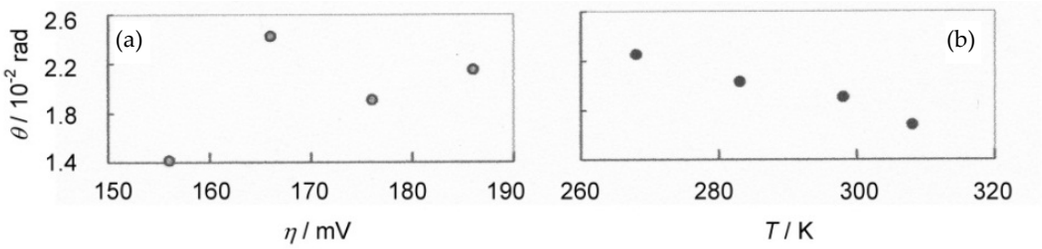

Figure 18. Inclination of surface to (111) face, which is given by $\theta^* = \tan^{-1}(v_{sm}/v_w)$.

α	ΔH_0/eV	v_{sm}/m s^{-1}	$\beta b/x_0$	v_{ed}/m s^{-1}	ΔG_{ed}*/eV	
					$K_s = 1$	$K_s = 0.2$
0.85	0.33	$1.6\times10^{-9\dagger}$	$0.034^\dagger$	$5.7\times10^{-9\dagger}$	$0.16^\dagger$	$0.12^\dagger$

†the value at 298K,

Table 3. Estimations of kinetics parameters controlling dissolution rate at edge dislocation site of surface of copper crystals.

4.3. Vertical dissolution rate at dislocation site

4.3.1. Estimation of the critical free energy change for nucleation of two-dimensional pit

As mentioned in Section 4.1.2 the dissolution rate v_{ed} at edge dislocation site is expressed by Eq. (23), but if Eq. (14) is applied it is reduced to

$$v_{ed} = aK_s C^0_{Cl^-}{}^{2(1-\alpha)} C^0_{CuCl_2^-}{}^{\alpha} \left(\left(\frac{C_{Cl^-}}{C^0_{Cl^-}} \right)^2 \right) \nu \exp\left(-\frac{\Delta G_{ed}{}^* + \Delta H_0 - \alpha n e \eta}{kT} \right). \tag{35}$$

Accordingly, if we assume $C_{Cl^-}/C^0_{Cl^-} \approx 1$, ΔG_{ed}^* is given by

$$\Delta G_{ed}^* \approx -kT\ln\left(\frac{v_{ed}}{aK_s C^{0\,2(1-\alpha)}_{Cl^-} C^{0\,\alpha}_{CuCl_2^-}\nu}\right) - \Delta H_0 + \alpha ne\eta. \tag{36}$$

Thus ΔG_{ed}^* under each condition was estimated by Eq.(36) with use of experimental value of v_{ed} as well as estimations of α and ΔH_0 which were obtained in Section 4.2.2. The ΔG_{ed}^* estimated with use of two assumed values of undetermined constant K_s for a specified condition (η = 176 mV and T = 298K) are shown together with the values α and ΔH_0 in Table 3, where $a = 2.09\times10^{-10}$ m and $\nu = 6.21\times10^{12}$ s^{-1} were used.

According to the precedent theoretical study (Schaarwächter 1965), in which the conditions for the formation of visible etch pit at dislocation site were investigated on the basis of a proposed nucleation model, the critical free energy change is estimated to be 0.115 eV. The present estimation of ΔG_{ed}^* approximately consists with that value as shown in Table 3, though the exact value of K_s can not be evaluated in this study. This is seemed to be reasonable as described in Appendix A2.

On the other hand, however, it was admitted that the value of ΔG_{ed}^* varies with overpotential and temperature as mentioned below.

4.3.2. Overpotential and temperature dependences of ΔG_{ed}^*

Figures 19 (a) and (b) are the diagrams that plotted the square root of ΔG_{ed}^* estimated assuming K_s = 1 by Eq. (36) against η and T respectively. It can be seen that $\Delta G_{ed}^{*1/2}$ is not constant but changes in different manners with increases in η and T. The reason for this is probably that $\Delta G_{ed}^{*1/2}$ is proportional to the interfacial energy γ as known from Eqs. (24) and (25).

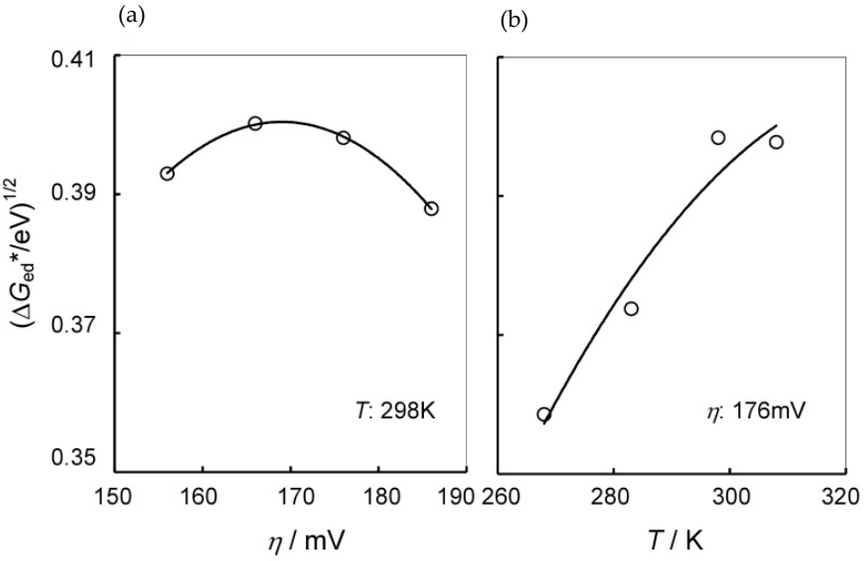

Figure 19. Square root of the critical free energy change for the formation of a two-dimensional pit. (a): The overpotential dependence; (b): The temperature dependence.

It is known that the interfacial energy varies with electrode potential according to so-called electrocapillary curve (Tamamushi, 1967). Therefore, the change in $\Delta G_{ed}^{*1/2}$ with η is surmised to be due to the potential dependence of γ, because the overpotential dependences of the undersaturation σ and therefore that of $\Delta\mu = ne\eta_a = -kT\ln(1-\sigma)$ in an overpotential range of 156 to 186 mV are assumed to be a little as described in Section 4.2.2. This is supported by the fact that Fig.19 (a) indicates a quadratic dependence similar to the electrocapillary curve. Also, it is inferred from Fig.19(b) and Eq.(24) that γ should increase with an increase in T, because $\Delta\mu$ tend to increase with increase in T. This is probably attributed to a decrease in specific adsorption of anion accompanied by an increase of interfacial energy with rising of temperature.

The overpotential dependence of log v_{ed} is in accelerative, and somewhat different from that of both log v_{sm} and log v_w. Also the increasing rate of log v_{ed} with increase in temperature is smaller than that of both log v_{sm} and log v_w as shown in Figs.14 (a) and (b). The reason for this seems to be attributed to the overpotential and temperature dependences of the interfacial energy of the electrode surface as mentioned above.

5. Conclusions

Following conclusions were obtained from the results and discussion:

1. The transfer coefficient, activation enthalpy and surface concentrations of the ions which control the dissolution reaction were estimated from measurements of the relationships between steady anodic current densities and applied overpotentials when copper crystals are dissolved in an electrolyte solution under potentiostatic electrolysis.
2. The values of a supplementary factor and kink density affecting rate constant of dissolution reaction were examined.
3. The dissolution rate at edge dislocation site of (111) surface of copper was discussed quantitatively by a nucleation model of two-dimensional pit based on the classical nucleation theory.
4. The present estimation of the critical free energy change ΔG_{ed}^* for nucleation of a two-dimensional pit at edge dislocation site reasonably consisted with the evaluation by the precedent study.
5. The overpotential and temperature dependences of dissolution rate at edge dislocation site were somewhat different from those dependences of dissolution rate at dislocation-free site. The reason for this is probably that ΔG_{ed}^* changes according to the overpotential and temperature dependences of interfacial energy.

6. Appendix

A1. Kinds of dislocation etch pits and their characters

The surface of copper specimen on which some small glass spheres 300 μm in diameter were dropped beforehand was anodically etched by the present method. Fig.20 (a) is an optical

micrograph of dissolved surface in which Rosseta pattern composed of dark and light etch pits was formed at the portion that was hit by a small glass sphere. This proves that dark and light etch pits are formed at the sites of positive and negative edge dislocations respectively because the six arms of Rosseta pattern are composed of rows of a pair of positive and negative edge dislocations.

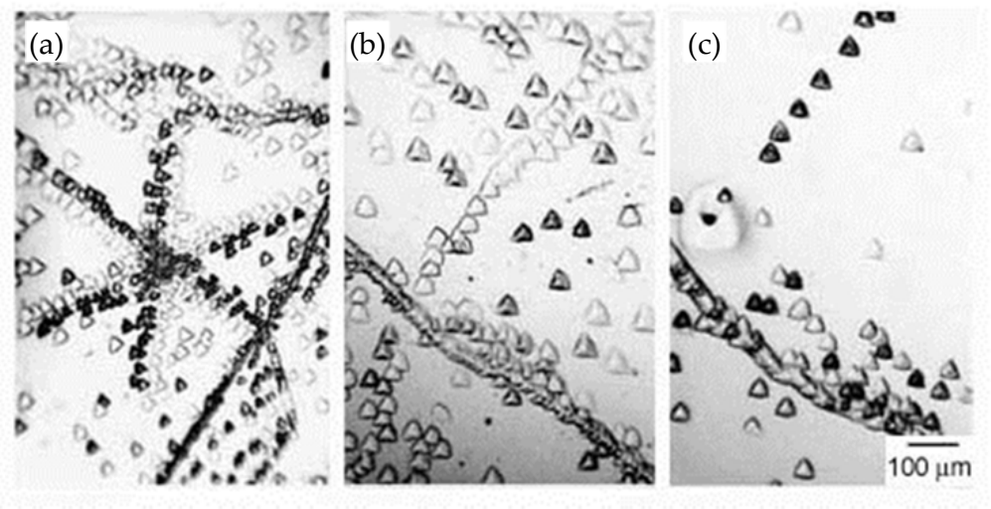

Figure 20. Optical micrographs for identifications of dark and light pits. The surfaces dissolved by the present method; (a): Rosetta pattern composed of etch pits; (b): a distribution of etch pits. (c): etch pits formed by a chemical etchant in the same portion as that observed in b.

In another experiment, the surface of prepared copper specimen was anodically etched first by the present method, and a distribution of etch pits were observed by the optical microscope. Subsequently after electropolished the etched surface of specimen, the surface was etched for 10 s by a modified Young's etchant prepared by Marukawa (Marukawa, 1967), and the same portion as the previous portion was observed. Figs.20 (b) and (c) are a pair of optical micrographs of the surfaces etched by such two methods. It has been reported by Marukawa that the dark (deep) and light (shallow) pits are formed at screw dislocations and edge dislocations on the surface etched by the modified Young's etchant respectively. Accordingly it can be seen that the light etch pits are formed at the sites of screw dislocations on the surface that was anodically etched by the present method, by comparing the kinds of etch pits which are observed in these micrographs. Thus Table 4 is obtained concerning dislocation characters related to dark and light etch pits.

Etching	Edge dislcation (positive)	(negative)	Screw dislcation
Chemical†	Light	Light	Dark
Electrolytic††	Dark	Light	Light

† by modified Young's etchant , †† present method

Table 4. Relations between the dislocation characters and the kinds of etch pits which are formed by two etching methods

In this work, the depth and width of the dark (deep) pits were measured to investigate the dissolution amounts at positive edge dislocation sites.

A2. Estimation of undetermined constant K_s

As described in the Section 4.1.3, if the separation rate r of an atom at nucleation of two-dimensional pit is a quantity similar to the dissolution rate of an atom from kink site of surface, it would need to take account of supplementary factor β affecting the exchange current density as a parameter involved in the separation rate r. Then the dissolution rate v_{ed} at edge dislocation site derived from the nucleation rate Eq. (21) is represented afresh by

$$v_{ed} \approx a\beta Z C_{Cl^-}{}^{2(1-\alpha)} C_{CuCl_2^-}{}^{\alpha} \nu \exp\left(-\frac{\Delta G_{ed}{}^{*} + \Delta H}{kT}\right). \tag{37}$$

Thus, we assume that the undetermined constant K_s is approximately given by a relation:

$$K_s = \beta Z. \tag{38}$$

We have assumed in the Section 2.7 that the exchange current density i_0 is given by Eq. (7) for simplification, but to be exact i_0 should be expressed with use of the activities of the ions involved in the electrode reaction instead of the concentrations. Also, transmission coefficient should be taken account of as pre-exponential factors in Eq. (7). Therefore it is generally hard to estimate β including some unknown factors. However, concerning β of the present electrode reaction, β (b/x_0) = 0.034 was estimated experimentally as shown in Table 3. Also it can be seen from an observation of etch pit by optical microscope that surface steps have a structure along a crystallographic direction of the crystal. Accordingly if (b/x_0) is assumed to be a quantity of 0.02 to 0.2, it would give an estimation of β = 0.17~1.7.

On the other hand, if we assume the free energy change ΔG_{ed} (j) for formation of a two-dimensional pit consisting of j vacancies at edge dislocation site, it is written as

$$\Delta G_{ed}(j) = 2\gamma\left(\pi a\Omega\right)^{1/2} j^{1/2} - \frac{\Delta\mu}{p'} j \tag{39}$$

Then the critical size j^* of two-dimensional pit and the critical free energy change $\Delta G_{ed}{}^*$(j^*) are given by

$$j^* = p'^2 \frac{\pi a\Omega\gamma^2}{\Delta\mu^2} \quad \text{and} \quad \Delta G_{ed}{}^*(j^*) = p' \frac{\pi a\Omega\gamma^2}{\Delta\mu} \tag{40}$$

respectively. It can be seen that $\Delta G_{ed}{}^*(j^*)$ is expressed by the same relation as Eq. (24), and that the factor p' has the same contents with Eq. (25), that is, $p' = p$. Then, Zeldovich factor is expressed from the definition (Toschev, 1973) by

$$Z = \sqrt{-\frac{1}{2\pi kT}\left(\frac{\partial^2 \Delta G_{ed}(j)}{\partial j^2}\right)_{j^*}} = \sqrt{\frac{1}{4\pi kT}\left(\frac{\Delta\mu^2}{p^2 \Delta G_{ed}{}^*}\right)}. \tag{41}$$

Accordingly, Z = 0.76 is estimated, if p = 0.18 (Schaarwächter 1965), $\Delta\mu$ = 0.027 eV(σ = 0.65) (Imashimizu, 2011), ΔG_{ed}^* = 0.12 eV (Table 3) and kT = 0.0257 eV (T = 298K) are used.

Thus K_s = 0.13~1.3 is estimated from Eq. (38), which suggests the reasonability of the assumed value of K_s shown in Table 3.

Author details

Yuji Imashimizu
Mineral Industry Museum, Faculty of Engineering and Resource Science, Akita University

Acknowledgments

The author thanks Emeritus Prof. Dr. J. Watanabé of Akita University for affording an opportunity to accomplish this study. He also wishes to express his thanks to Messrs.T. Wakayama and Y. Hirai, who carried out much of experimental work.

7. References

Burton, W. Cabrera, N. & Frank, F. (1951). The Growth of Crystals and the Equilibrium Structure of their Surfaces, *Philosophical Transactions of the Royal Society,* A 243, pp.299-358.

Cabrera, N. & Levine, M. (1956), On the Dislocation Theory of Evaporation of Crystals, *Philosophical Magazine*, Vol. 1, pp. 450-458.

Despic, A. & Bockris, J. (1960), Kinetics of the Deposition and Dissolution of Silver, *The Journal of Chemical Physics*, Vol. 32, No.2, pp. 389-402.

Gilman, J., Johnston, W. & Sears, G. (1958), Dislocation Etch Pit Formation in Lithium Fluoride, *Journal of Applied Physics* Vol.29, No. 5, pp.747- 754

Imashimizu, Y. & Watanabé, J. (1983), Dissolution Rate at Dislocations on a (111) Surface of Copper Crystal under Potentiostatic Electrolysis, *Transactions of The Japan Institute of Metals*, Vol. 24, No.12, pp.791-798.

Imashimizu,Y. (2010), Dissolution Rate of the (111) Surface of Copper Crystals under Potentiostatic Electrolysis, *Journal of the JRICu*, Vol. 49, No.1, ISSN 1347-7234, pp. 258-263. (in Japanese).

Imashimizu, Y. (2011), Dissolution kinetics at edge dislocation site of (111) surface of copper crystals, *Journal of Crystal Growth*, Vol. 318, pp.125-130.

Ives, M. & Hirth, J. (1960), Dissolution Kinetics at Dislocation Etch Pits in Single Crystals of Lithium Fluoride, *The Journal of Chemical Physics*, Vol.33, No. 2, pp.517-525.

Jasper, L & Schaarwächter, W. (1966), Ätzgrubenbildung an Versetzungen in Kupfereinkristallen durch potentiostatische Elektrolyse, *Zeitschrift für Metallkunde*, Bd. 57, H. 9, pp.661-668.

Lal, H. & Thirsk, H. (1953), The Anodic Behaviour of Copper in Neutral and Alkaline Chloride Solutions, *Journal of Chemical Society*, pp. 2638-2644.

Lee, H. & Ken Nobe (1986), Kinetics and Mechanism of Cu Electrodissolution in Chloride Media, *Journal of Electrochemical Society*, Vol. 133, No. 10, pp.2035-2043.

Maeda, M. (1961), *Denkyoku No Kagaku*, Gihodo, ASIN: B000JAMTNW, Tokyo, Japan (in Japanese)

Marukawa, K. (1967), Dark and Light Pits on (111) Surface of Copper, *Japanese Journal of applied Physics*, Vol. 6, No. 8. pp.944-949.

Onuma, K., Tsukamoto, K. & Sunagawa, I. (1991), Dissolution kinetics of K-alum crystals as judged from the measurements of surface undersaturations, *Journal of Crystal Growth*, Vol. 110, pp.724-732.

Schaarwächter, W. (1965), Zum Mechanismus der Versetzungsätzung, I. Die Bildung zweidimensionaler Lochkeime an den Enden von Versetzungslinien, *physica status solidi*, Bd. 12, pp. 375-382.

Schaarwächter, W. (1965), Zum Mechanismus der Versetzungsätzung II Entstehungsbedingungen für Atzgruben, *physica status solidi*, Bd. 12, pp. 865- 876.

Schaarwächter , W. & Lücke, K. (1967), Der Einfluβ der versetzungsstruktur auf die Auflösung von Kristallen, *Zeitschrift für Physikalische Chemie Neue Folge*, Bd. 53, pp. 367-386.

Tamamushi, R. (1967), *Denkikagaku*, Tokyo Kagaku Doujin, NCID: BN01795418, Tokyo, Japan (in Japanese)

Toschev, S. (1973), Homogeneous nucleation, In: *Crystal Growth: An Introduction*, P. Hartman, (Ed.), 1-49. ISBN North-Holland 0 7204 1821 6 / ISBN American Elsevier 0444 10463 1, Amsterdam

Van Der Hoek, B.;Van Enckevort, W. & Van Der Linden, W. (1983), Dissolution Kinetics and Etch Pit Studies of Potassium Aluminium Sulphate, *Journal of Crystal Growth*, Vol.61, pp.181-193.

Watanabé, J.; Imashimizu, Y. & Sugawara, S. (2003), Dissolution Kinetics at Dislocation Site of Copper Crystal, *Journal of the Society of Materials Engineering for Resources of Japan*, Vol. 16, No. 1, pp.13-20. (in Japanese).

Young, Jr., F. (1961), Etch Pits at Dislocations in Copper, *Journal of Applied Physics*, Vol. 32, No. 2, pp. 192-201.